

# Data classification based on the local intrinsic dimension

Michele Allegra<sup>1,2</sup>, Elena Facco<sup>1</sup>, Francesco Denti<sup>3,5</sup>, Alessandro Laio<sup>1,4,\*</sup>, and Antonietta Mira<sup>5,6,+</sup>

<sup>1</sup>Scuola Internazionale Superiore di Studi Avanzati, Trieste, Italy

<sup>2</sup>Institut de Neurosciences de la Timone UMR 7289, Aix Marseille Université, CNRS, 13385 Marseille, France

<sup>3</sup>University of Milan Bicocca, Milan, Italy

<sup>4</sup>International Centre for Theoretical Physics, Trieste, Italy

<sup>5</sup>Università della Svizzera italiana, Lugano, Switzerland

<sup>6</sup>Università dell'Insubria, Como, Italy

\*laio@sissa.it

+antonietta.mira@usi.ch

## ABSTRACT

One of the founding paradigms of machine learning is that a small number of variables is often sufficient to describe high-dimensional data. The minimum number of variables required is called the intrinsic dimension (ID) of the data. Contrary to common intuition, there are cases where the ID varies within the same data set. This fact has been highlighted in technical discussions, but seldom exploited to analyze large data sets and obtain insight into their structure. Here we develop a robust approach to discriminate regions with different local IDs and classify the points accordingly. Our approach is computationally efficient, and can be profitably used even on large data sets. We find that many real-world data sets contain regions with widely heterogeneous dimensions. These regions host points differing in core properties: folded vs unfolded configurations in a protein molecular dynamics trajectory, active vs non-active regions in brain imaging data, and firms with different financial risk in company balance sheets. A simple topological feature, the local ID, is thus sufficient to achieve an unsupervised classification of high-dimensional data, complementary to the one given by clustering algorithms.

## Introduction

From string theory to science fiction, the idea that we might be “glued” onto a low-dimensional surface embedded in a space of large dimensionality has tickled the speculations of scientists and writers alike. When it comes to multidimensional data, however, such situation is quite common rather than a wild speculation: data often concentrate on hypersurfaces of low *intrinsic dimension* (ID). Estimating the ID of a dataset is a routine task in machine learning: it yields important information on the global structure of a dataset, and is a necessary preliminary step in several analysis pipelines.

In most approaches for dimensionality reduction and manifold learning the ID is assumed to be constant in the dataset. This assumption is implicit in projection-based estimators, such as Principal Component Analysis (PCA) and its variants<sup>1</sup>, Locally Linear Embedding<sup>2</sup>, and Isomap<sup>3</sup>; and it also underlies geometric ID estimators<sup>4-6</sup>, which infer the ID from the distribution of between points distances. The hypothesis of a constant ID complies with simplicity and intuition, but is not necessarily valid. In fact, many authors have considered the possibility of ID variations within a dataset<sup>7-22</sup>, often proposing to classify the data according to this feature. However the dominant opinion in the community is still that a variable ID is a peculiarity, or a technical detail, rather than a common feature to take into account before performing a data analysis. This perception is in part due to the lack of sufficiently general and Big-Data-compliant methods to track ID variations. Many of the methods developed in this field make assumptions that limit their applicability to specific classes of data. Refs.<sup>7,11-14</sup> use local ID estimators that implicitly or explicitly assume a uniform density. Refs.<sup>8-10</sup> jointly estimate the density and the ID from the scaling on the neighbor distances, by approaches which work well only if the density varies slowly and is approximately constant in a large neighborhood of each point. Ref.<sup>15</sup> requires a priori knowledge on the number of manifolds and on their IDs. Refs.<sup>16-18,20</sup> all require that the manifolds on which the data lay are hyperplanes, or topologically isomorphic to hyperplanes. These assumptions (locally constant density, and linearity in a suitable set of coordinates) are quite strong in the case of real-world data. Moreover, many of the above approaches<sup>7,11-13,15-20</sup> work explicitly with the coordinates of the data, while in many applications only distances between pairs of data points are available. To our knowledge, only refs.<sup>21,22</sup> do not make any assumption about the density, as they derive a parametric form of the distance distribution using extreme-value theory, which in

principle is valid independently of the form of the underlying density. However, they assume that the low tail of the distance distribution is well approximated by its asymptotic form, an equally non-trivial assumption.

In this work we propose a method to classify data based on the local ID which aims at overcoming all the aforementioned limitations. Building on TWO-NN<sup>23</sup>, a recently proposed ID estimator which is insensitive to density variations and uses only the distances between points, we develop a Bayesian framework which allows identifying, by Gibbs sampling, the regions in the data landscape in which the ID can be considered constant. Our approach works even if the data are embedded on highly curved and twisted manifolds, if the manifolds are topologically complex and not isomorphic to hyperplanes and if the probability density, from which the data are harvested, is non-uniform. Moreover, it is specifically designed to use only the distance between data points, and not their coordinates. These features, as we will show, make our approach computationally efficient and more robust than other methods. Applying our approach to data of various origin, we show that ID variations between different regions are common. These variations often reveal fundamental properties of the data: for example, unfolded states in a molecular dynamics trajectory of a protein fall on a manifold of a lower dimension than the one hosting the folded states. Identifying regions of different dimensionality in a dataset can thus be a way to perform an unsupervised classification of the data. At odds with common approaches, we do not group the data according to their density, but perform classification based on a geometric property defined on a local scale: the number of independent directions along which neighbouring data are spread.

## Results

### *A Bayesian approach for discriminating manifolds with different ID*

The starting point of our approach is the recently proposed TWO-NN estimator<sup>23</sup>, which infers the IDs from the statistics of the distances of the first two neighbors of each point. Let the data  $(x_1, x_2, \dots, x_N)$ , with  $N$  the number of points, be i) independent and identically distributed samples from a probability density  $\rho(x)$  with support on a manifold with unknown dimension  $d$ , such that ii) for each point  $x_i$ ,  $\rho(x_i)$  is approximately constant in the spherical neighborhood with center  $i$  and radius given by the distance between  $i$  and its second neighbor. Assumption i) is shared all methods that infer the ID from the distribution of distances (e.g., Refs.<sup>5,6,9-12,14</sup>. Assumption ii) is the key assumption of TWO-NN: while of course it may not be perfectly satisfied, other methods to infer the ID from distances require uniformity of the density on a larger scale including the first  $k$  neighbors, usually with  $k \gg 2$ . Let  $r_{i1}$  and  $r_{i2}$  be the distances of the first and second neighbor of  $x_i$ , then  $\mu_i \doteq \frac{r_{i2}}{r_{i1}}$  follows the Pareto distribution  $f(\mu_i|d) = d\mu_i^{-(d+1)}$ . This readily allows the estimation of  $d$  from  $\mu_i, i = 1, 2, \dots, N$ . We can write the global likelihood of  $\mu \equiv \{\mu_i\}$  as

$$P(\mu|d) = d^N \prod_{i=1}^N \mu_i^{-(d+1)} = d^N e^{-(d+1)V}, \quad (1)$$

where  $V \doteq \sum_{i=1}^N \log(\mu_i)$ . We here assume that the variables  $\mu_i$  are independent. This condition can be rigorously imposed by restricting the product in eq. 1 to data points with no common first and second neighbor. In all data sets we studied, we never found significant differences between the distribution of  $\mu$  obtained with all points and the one obtained by restricting to independent triples. Therefore, for purposes of parametric inference we simply include all points in the estimation. From Eq. (1), and upon specifying a suitable prior on  $d$ , a Bayesian estimate of  $d$  is immediately obtained. In<sup>23</sup>, it was shown that restricting the uniformity requirement only to the region containing the first two neighbors allows properly estimating the ID also in cases where the density  $\rho$  is strongly varying.

TWO-NN can be extended to yield a heterogeneous-dimensional model with an arbitrarily high number of components. Let  $x = \{x_i\}$  be i.i.d samples from a density  $\rho(x)$  with support on the union of  $K$  manifolds with varying dimensions. This multi-manifold framework is common with many previous works investigating heterogeneous dimension in a dataset<sup>8-11,14-16,18-20,24,25</sup>. Formally, let  $\rho(x) = \sum_{k=1}^K p_k \rho_k(x)$  where each  $\rho_k(x)$  has support on a manifold of dimension  $d_k$  and  $p \doteq (p_1, p_2, \dots, p_K)$  are the a priori probabilities that a point belongs to the manifolds  $1, \dots, K$ . We shall first assume that  $K$  is known, and later show how it can be estimated from the data. The distribution of the  $\mu_i$  is simply a mixture of Pareto distributions:

$$P(\mu_i|d, p) \doteq \sum_{k=1}^K p_k d_k \mu_i^{-(d_k+1)}. \quad (2)$$

Following the customary approach<sup>26</sup> we introduce latent variables  $z \doteq (z_1, z_2, \dots, z_K)$  where  $z_i = k$  indicates that point  $i$  belongs to manifold  $k$ . We have  $P(\mu_i|d, p, z) = P(\mu_i|z_i, d)P_{pr}(z_i|p)$  with  $P(\mu_i|z_i, d) = d_{z_i} \mu_i^{-(d_{z_i}+1)}$ ,  $P_{pr}(z_i|p) = p_{z_i}$ . This yields the posterior

$$P_{post}(z, d, p|\mu) \propto P(\mu|z, d)P_{pr}(z|p)P_{pr}(d)P_{pr}(p). \quad (3)$$

We use independent Gamma priors on  $d$ ,  $d_k \sim \text{Gamma}(a_k, b_k)$  and a joint Dirichlet prior on  $p \sim \text{Dir}(c_1, \dots, c_K)$ . We fix  $a_k, b_k, c_k = 1 \forall k$ , corresponding to a maximally non-informative prior on the  $p$  and an expectation of  $d_k = 1$  for all  $k$ . If one has different a priori expectation on  $d$  and  $p$ , other choices of prior may be more convenient.

The posterior (3) does not have an analytically simple form, but it can be sampled by standard Gibbs sampling<sup>27</sup>, allowing for the joint estimation of  $d, p, z$ . Model (3) has, however, a serious limitation: Pareto distributions with (even largely) different values of  $d$  overlap to a great extent. Therefore, the method can not be expected to correctly estimate the  $z_i$ : a given value  $\mu_i$  may be compatible with several manifold memberships. This issue can be addressed by correcting an unrealistic feature of model (3), namely, the independence of the  $z_i$ . We assume that the neighborhood of a point is more likely to contain points from the same manifold than from different manifolds. This requirement can be enforced with an additional term in the likelihood that penalizes local inhomogeneity (see also Ref. 14). Consider the  $q$ -neighbor matrix  $\mathcal{N}^{(q)}$  with nonzero entries  $\mathcal{N}_{ij}^{(q)}$  only if  $j \neq i$  is among the first  $q$  neighbors of  $i$ . Let  $\zeta$  be the probability to sample the neighbor of a point from the same manifold, and  $1 - \zeta$  the probability to sample it from a different manifold, with  $\zeta > 0.5$ . Define  $n_i^{\text{in}}$  as the number of neighbors of  $i$  with the same manifold membership ( $n_i^{\text{in}} \equiv \sum_j \mathcal{N}_{ij}^{(q)} \delta_{z_i z_j}$ ). Then we introduce a probability distribution for  $\mathcal{N}^{(q)}$  as:

$$P(\mathcal{N}^{(q)}|z) = \prod_{i=1}^N \frac{\zeta^{n_i^{\text{in}}} (1 - \zeta)^{q - n_i^{\text{in}}}}{\mathcal{Z}(\zeta, N_{z_i})} \quad (4)$$

where  $\mathcal{Z}_q$  is a normalization factor that depends also on the sizes of the manifolds (see SI for its explicit expression). This term favors homogeneity within a  $q$ -neighborhood of each point. With this addition, the model now reads:

$$P_{\text{post}}(z, d, p | \mu, \mathcal{N}^{(q)}) \propto P(\mu | z, d) P(\mathcal{N}^{(q)} | z) P_{\text{pr}}(z | p) P_{\text{pr}}(d) P_{\text{pr}}(p). \quad (5)$$

The posterior (5) is sampled with Gibbs sampling starting from a random configuration of the parameters. The parameters  $d$  and  $p$  can be estimated by their posterior averages. For all estimations, we only include the last 10% of the points. This ensures that the initial burn-in period is not excluded, and ensures that we do not incur in label switching issues<sup>28</sup>. Indeed, once the chains converge to one mode of the posterior distribution they do not transition to different modes. As for the  $z$ , we estimate the value of  $\pi_{ik} \equiv P_{\text{post}}(z_i = k)$ . Point  $i$  can be safely assigned to manifold  $k$  if  $\pi_{ik} > 0.8$ , otherwise we will consider its assignment to be uncertain. We repeat the sampling  $M$  times starting from different random configurations of the parameters, keeping the chain with highest maximum log-posterior value.

We name our method Hidalgo (Heterogeneous Intrinsic Dimension Algorithm). Hidalgo has three free parameters: the number of manifolds,  $K$ ; the local homogeneity range, denoted by  $q$ ; the local homogeneity level, denoted by  $\zeta$ . We fix  $q$  and  $\zeta$  based on preliminary tests conducted on artificial data sets (see SI). As is common for mixture models, the value of  $K$  can be estimated by model selection. In particular, we can compare the models with  $K$  and  $K + 1$  for increasing  $K$ , starting from  $K = 1$  and stopping when there is no longer significant improvement, as measured by the average log-posterior. The code implementing the method is freely available on <https://github.com/micheleallegra/Hidalgo>.

### Validation of the method on artificial data

We first tested Hidalgo on artificial data for which the true manifold partition of the data is known. We start from the simple case of two manifolds with different ID,  $d_1$  and  $d_2$ . We consider several examples, fixing the lower dimension  $d_1$  to 4 and varying the higher dimension  $d_2$  from 5 to 9. On either manifold,  $N = 1000$  points are sampled from a multivariate Gaussian with a variance matrix given by  $1/d_i$ ,  $i = 1, 2$ , times the identity matrix of proper dimension. The two manifolds are embedded in a space with dimension corresponding to the higher dimension  $d_2$ , with their centers at a distance of 0.5 standard deviations, so they are partly overlapping. In Fig. 1a-b we illustrate the results obtained in the case of fixed  $\zeta = 0.5$ , equivalent to the absence of any statistical constraint on neighborhood uniformity. The estimate of the two dimensions is shown together with the mutual information (MI) between the estimated assignment of points and the true one. As expected, without a constraint on the assignment of neighbors, the method is not able to correctly separate the points and thus to estimate the dimensions of the two manifolds, even in the case of quite different ID. As soon as we take  $\zeta > 0.5$ , results improve. A detailed analysis on the influence of the hyperparameters  $q$  and  $\zeta$  is reported in SI. On the basis of such analysis, we identify the following as good parameter ranges:  $q \in \{3, 4, 5\}$  and  $\zeta \in [0.7, 0.85]$ . In Fig. 1c-d we repeat the same tests as in 1a-b but with  $q = 3$  and  $\zeta = 0.8$ . Now the MI between the estimated and ground truth assignment is almost 1 in all cases and correspondingly the estimation of  $d_1$  and  $d_2$  is accurate. To verify whether our approach is able to discriminate between more than two manifolds ( $K > 2$ ), we consider a more challenging dataset consisting of five Gaussians with unitary variance in dimensions 1, 2, 4, 5, 9 respectively. Some of the Gaussians have similar IDs, as in the case of dimensions 1 and 2, or 4 and 5; moreover they can be very close to each other, for instance the centers of those in dimensions 4 and 5 are only half a variance far from each other, and they are

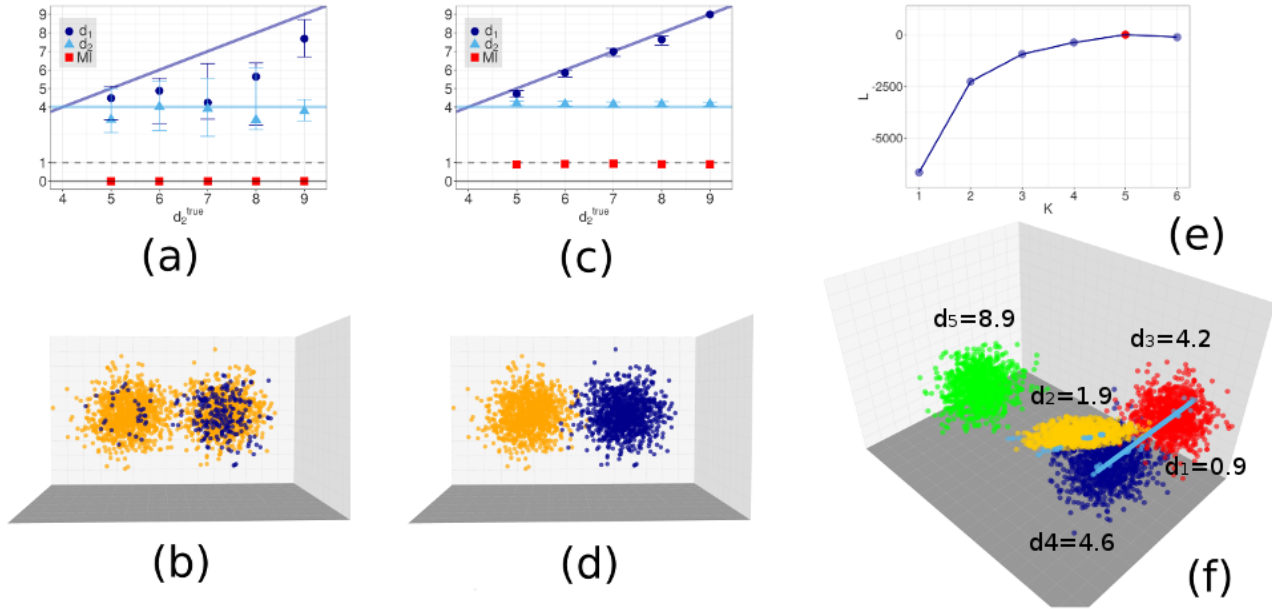


**Figure 1. Results on simple artificial data sets.** We considered sets of points drawn from mixtures of multivariate Gaussians in different dimensions. In all cases, we performed  $10^5$  iterations of the Gibbs sampling, and repeated the sampling  $M = 10$  times starting from different random configurations of the parameters. We kept the sampling with highest maximum average of the log-posterior value. **Panels a)-b):** Points drawn from two Gaussians in different dimensions. The lower dimension is fixed at  $d_1 = 4$ , the higher varies from  $d_2 = 5$  to  $d_2 = 9$ .  $N = 1000$  points are sampled from each manifold. We show results obtained with  $\zeta = 0.5$ , namely, without enforcing neighborhood uniformity (here  $q = 1$ , but since  $\zeta = 0.5$  the value of  $q$  is irrelevant). In panel a) we plot the estimated dimensions of the manifolds (dots: posterior means; errorbars: posterior standard deviations) and the MI between our classification and the ground truth. In panel b) we show the assignment of points to the low-dimensional (blue) and high-dimensional (orange) manifold (points are projected onto the first 3 coordinates). **Panels c)-d):** The same setting as in panels a)-b), but now we enforce neighborhood uniformity, using  $\zeta = 0.8$  and  $q = 3$ . Points are now correctly assigned to the manifolds whose ID is properly estimated. **Panels e)-f):** Points drawn from five Gaussians in dimensions  $d_1 = 1, d_2 = 2, d_3 = 4, d_4 = 5, d_5 = 9$ .  $N = 1000$  points are sampled from each manifold. Some pairs of manifolds are intersecting, as their centers are one standard deviation apart. The analysis is performed with  $\zeta = 0.8, q = 3$  and with different values of  $K$ . In panel e) we show the average log-posterior value  $\mathcal{L}$  as a function of  $K$ . The maximum  $\mathcal{L}$  corresponds to the ground truth value  $K = 5$ . In panel f) we show the assignment of points to the five manifolds in different colors (points were projected onto the first 3 coordinates).

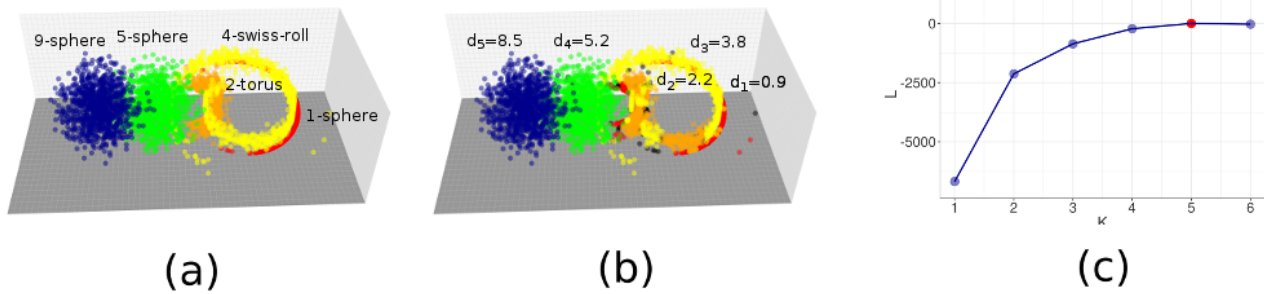


**Figure 2. Results on data sets on curved manifolds.** We considered sets of points drawn from mixtures of multivariate Gaussians embedded in curved nonlinear manifolds: a 1-dimensional circle, a 2-dimensional torus, a 4-dimensional Swiss roll, a 5-dimensional sphere and a 9-dimensional sphere. All the manifolds are embedded in a 9-dimensional space.  $N = 1000$  points are sampled from each manifold. Some pairs of manifolds are intersecting. In all cases, we performed  $10^5$  iterations of the Gibbs sampling, and repeated the sampling  $M = 10$  times starting from different random configurations of the parameters. We kept the sampling with highest maximum log-posterior value. The analysis is performed with  $\zeta = 0.8$ ,  $q = 3$  and with different values of  $K$ . In panel a we show the ground-truth assignment of points to the five manifolds in different colors (points were projected onto the first 3 coordinates). In panel b) we show the assignment of points as given by Hidalgo with  $K = 5$ . In panel c) we show the average log-posterior value  $\mathcal{L}$  as a function of  $K$ . The maximum  $\mathcal{L}$  corresponds to the ground truth value  $K = 5$ .

crossed by the Gaussian in dimension 1. To analyze such dataset we again choose the hyperparameters  $q = 3$  and  $\zeta = 0.8$ . We do not fix the number of manifolds  $K$  to its ground truth value  $K = 5$ , but we try to let the method estimate  $K$  without relying on a priori information. We perform the analysis with different values of  $K = 1, \dots, 6$  and compute an estimate of the average of the logarithm of the posterior value  $\mathcal{L}$  for each  $K$ . Results are shown in Fig. 1e. We see that  $\mathcal{L}$  increases up to  $K = 5$ , and then decreases, from which we infer that the optimal number of manifolds is  $K = 5$ . In Fig. 1f we illustrate the final assignment of points to the respective manifolds together with the estimated dimensions, upon setting the number of manifolds to  $K = 5$ . The separation of the manifolds is very good. Only a few points of the manifold with dimension 1 are incorrectly assigned to the one with dimension 2 and vice versa. The values of normalized mutual information between the ground truth and our classification is 0.89.

Finally, we show that our method can handle data embedded in curved manifolds, or with complex topologies. Such data should not pose additional challenges to the method. Indeed Hidalgo is sensitive only to the local structure of data. In terms of the distribution of the first and second nearest-neighbor distances, a 2-d torus looks exactly like a 2-d plane, and thus we should be able to correctly classify these objects, that are so topologically different, as 2-d objects regardless of their shape. We generated a dataset with 5 Gaussians in dimension 1, 2, 4, 5, 9 (Fig. 2a). Each Gaussian is then embedded on a curved nonlinear manifold: a 1-dimensional circle, a 2-dimensional Swiss roll, a 4-dimensional Swiss roll, a 5-dimensional sphere and a 9-dimensional sphere. All manifolds are topologically not isomorphic to a hyperplane, except for the Swiss roll. Moreover, the manifolds are intersecting. As shown in Fig. 2b, our approach is able to discriminate the five manifolds. The dimension are correctly retrieved (Fig. 2c), points are assigned to the right manifold with an accuracy corresponding to a normalized mutual information (NMI) = 0.83. Only some points of the 3d-torus are misassigned to the 4d-swiss roll.

### **ID variability in a protein folding trajectory**

As a first real application of Hidalgo, we address ID estimation for a dynamical system. Asymptotically, dynamical systems are usually restrained to a low-dimensional manifold in phase space, called an attractor. Much effort has been devoted to characterizing the ID of such attractor<sup>4</sup>. However, in the presence of multiple metastable states an appropriate description of the visited phase space may require the use of multiple IDs. Here, we consider the dynamics of the villin headpiece (PDB entry: 2F4K). Due to its small size and fast folding kinetics, this small protein is a prototypical system for molecular dynamics simulations. Our analysis is based on the longest available simulated trajectory of the system from Ref.<sup>31</sup>. During the simulated  $125 \mu s$ , the protein performs approximately 10 transitions between the folded and the unfolded state. We expect to find different dimensions in the folded and unfolded state, since these two states are metastable, and they would be considered as different attractors in the language of dynamical systems. Moreover, they are characterized by different chemical and physical features: the folded state is compact and dry in its core, while the unfolded state is swollen, with most of the residues interacting with a large number of water molecules. We extract the value of the 32 key observables (the backbone dihedral angles) for all the  $N = 31,000$  states in the trajectory and apply Hidalgo to this data of extrinsic dimension  $D = 32$ . We obtain a vector of estimated intrinsic dimensions  $d$  and an assignment of each point  $i$  to one of the  $K$  manifolds. We find four manifolds, three

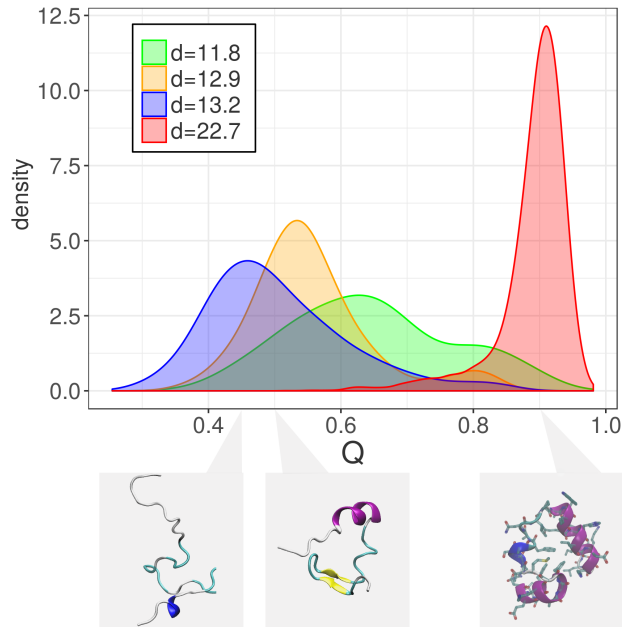


**Figure 3. Protein folding trajectory.** We considered  $N \sim 31,000$  configurations of a protein undergoing successive folding/unfolding cycles. For each configuration, we extracted the value of the  $D = 32$  backbone dihedral angles. Applying Hidalgo to these data, we found four manifolds, of intrinsic dimensions 11.8, 12.9, 13.2 and 22.7. For each configuration, we also computed the fraction of native contacts,  $Q$ , which measures to which degree the configuration is folded. The figure shows the probability distribution of  $Q$  in each manifold. Nearly all the folded configurations belong to the high-dimensional manifold: the analysis essentially identifies the folded configurations as a region of high intrinsic dimension. Results were obtained with  $q = 3$  and  $\zeta = 0.8$ . The distance between each pair of configurations was computed by the Euclidean metric with periodic boundary conditions on the vectors of the dihedral angles.

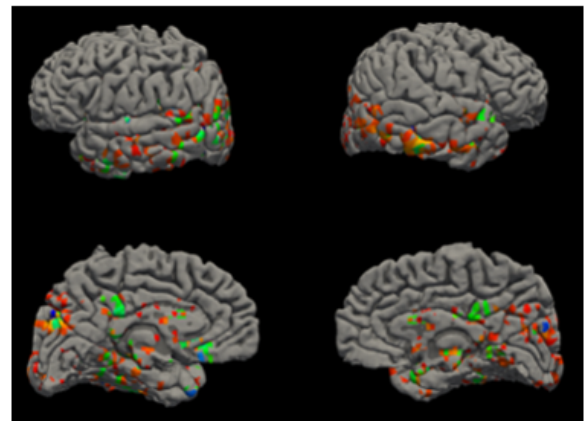
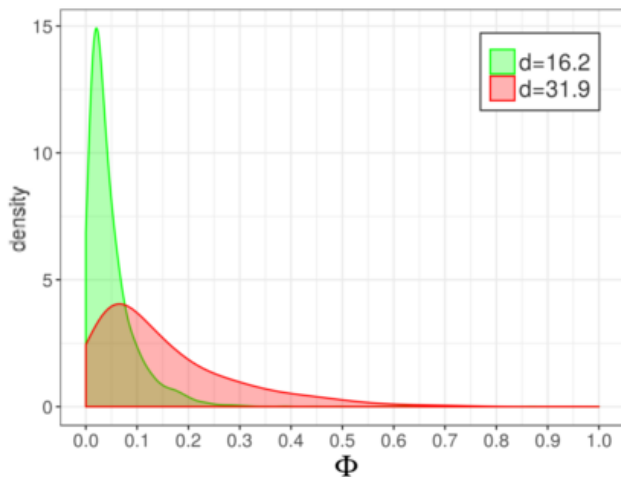


**Figure 4. Neuroimaging data.** We considered the BOLD time series of  $N \sim 30,000$  voxels in an fMRI experiment with  $D = 202$  scans. Hidalgo found a low-dimensional manifold ( $d = 16.2$ ) and a high-dimensional one ( $d = 31.9$ ). We computed the clustering frequency  $\Phi$ , which measures the participation of each voxel to coherent activation patterns and is a proxy for voxel involvement in the task<sup>29</sup>. (Top) probability distribution of  $\Phi$  in the two manifolds. Strongly activated voxels ( $\Phi > 0.2$ ) are consistently assigned to the high-dimensional manifold. (Bottom) rendering of the cortical surface (left: left hemisphere; right: right hemisphere). Blue voxels have high clustering frequency ( $\Phi > 0.2$ ), red voxels are those assigned to the high-dimensional manifold, and green voxels satisfying both criteria. Almost all voxels with high clustering frequency are assigned to the high-dimensional manifold, and are concentrated in the occipital, temporal and parietal cortex. Results were obtained with  $q = 3$  and  $\zeta = 0.8$ . The distance between two time series was computed by a Euclidean metric, after standard pre-processing steps<sup>30</sup>.

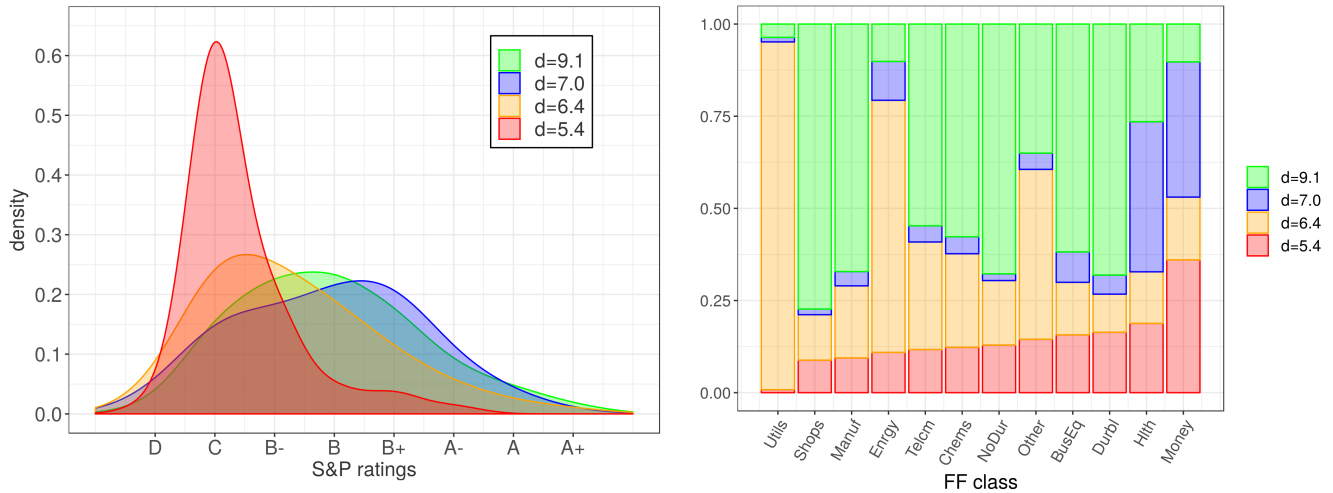


**Figure 5. Financial data.** For  $N \sim 8,000$  firms selected from the COMPUSTAT database, we computed  $D = 31$  variables from their yearly balance sheets. Hidalgo finds four manifolds of intrinsic dimensions 5.4, 6.4, 7.0 and 9.1. (Top) fraction of firms assigned to the four manifolds for each type of firm, according to the Fama-French classification. The four manifolds contain unequal proportions of firms belonging to different classes, implying that some classes of firms are preferentially assigned to manifolds of high vs low dimension. (Bottom) probability distribution of the S&P ratings of the firms assigned to each manifold. Firms with low ratings preferentially belong to low-dimensional manifolds. Results were obtained with  $q = 3$  and  $\zeta = 0.8$ . To correct for firm size, we divided the variable vector of each firm by its norm, and then applied standard Euclidean metric.

low-dimensional ones ( $d_1 = 11.8$ ,  $d_2 = 12.9$ ,  $d_3 = 13.2$ ) and a high-dimensional one ( $d_4 = 22.7$ ). Note that two spatially separated regions with approximately the same dimension (in this case,  $d_2$  and  $d_3$ ) are recognized as distinct manifolds by our approach. To test whether this partition into manifolds is related to the separation between the folded and the unfolded state we relate the partition to the fraction of native contacts  $Q$ , which can be straightforwardly estimated on each configuration of the system.  $Q$  is close to one only if the configuration is folded, while it approaches zero when the protein is unfolded. In Fig. 3 we plot the probability distribution of  $Q$  restricted to the four manifolds. We find that the vast majority of the folded configurations ( $Q > 0.8$ ) are assigned to the high-dimensional manifold. Conversely, the unfolded configurations ( $Q < 0.7$ ) are most of the times assigned to one of the low-dimensional manifolds. This implies that a configuration belonging to the low dimensional manifolds is almost surely unfolded. Thus, we can essentially identify the folded state using the intrinsic dimension, a purely topological observable unaware of any chemical detail.

#### ID variability in time-series from brain imaging

In the next example, we analyze a set of time-series from functional resonance imaging (fMRI) of the brain, representing the BOLD (blood oxygen-level dependent) signal of each voxel, which captures the activity a small part of the brain<sup>32</sup>. fMRI time-series are often projected on a lower dimension through linear projection techniques like PCA<sup>33</sup>, a step that assumes a uniform ID. However, the gross features of the signal (e.g., power spectrum and entropy) are often highly variable in different parts of the brain, and also non-uniformities in the ID may well be present. Here, we consider a single-subject fMRI recording containing  $D = 202$  images collected while a subject was performing a visuomotor task<sup>29,34</sup>. From the images we extracted the  $N = 29851$  time series corresponding to the BOLD signals of each voxel. Applying our Hidalgo, we find two manifolds with very different dimensions  $d_1 = 16.2$ ,  $d_2 = 31.9$ . Again, we relate the identified manifolds to a completely independent quantity, the clustering frequency  $\Phi$  introduced in<sup>29,30</sup>, which measures the temporal coherence of the signal of a voxel with the signals of other voxels in the brain. Voxels with non-negligible clustering frequency ( $\Phi > 0.2$ ) are likely to belong to brain areas involved in the cognitive task at hand. In Fig. 4 we show the probability distribution of  $\Phi$  restricted to the two manifolds. We find that the “task-related” voxels ( $\Phi > 0.2$ ) almost invariably belong to the manifold with high dimensionality. These voxels appear concentrated in the occipital, parietal and temporal cortex (Fig. 4 bottom), and belong to a task-relevant network of coherent activity<sup>29</sup>. This result finds a natural and appealing interpretation: the subset of “relevant” voxels give rise to patterns that are not only coherent, but also characterized by a larger ID than the remainder of the voxels. On the contrary, the incoherent voxels exhibit a lower ID, hence a reduced variability, which is consistent with the fact that the corresponding time series are dominated by low-dimensional noise. Again, this feature emerges from the global topology of the data, revealed by our ID

analysis, without exploiting any knowledge of the task that the subject is performing.

### ***ID variability in financial data***

Our final example is in the realm of economics. We considered firms in the well-known Compustat database ( $N = 8309$ ). For each firm, we consider  $D = 31$  balance sheet variables from the fiscal year 2016 (for details, see Table 1 in the SI). Applying Hidalgo we find four manifolds of dimensions  $d_1 = 5.4$ ,  $d_2 = 6.3$ ,  $d_3 = 7.0$  and  $d_4 = 9.1$ . To understand this result, we try to relate our classification with common indexes showing the type and financial stability of a firm. We start by relating our classification to the Fama-French classification<sup>35</sup>, which assigns each firm to one of twelve categories depending on the firm's trade. In Fig. 5(top) we separately consider firms belonging to the different Fama-French classes, and compute the fraction of firms assigned to each the four manifolds identified by Hidalgo. The two classifications are not independent, since the fractions for different Fama-French classes are highly non-uniform. More precisely, the mutual information (MI) between the two classifications is 0.19, rejecting hypothesis of statistical independence ( $p$ -value  $< 10^{-5}$ ). In particular, firms in the utilities and energy sector show a preference for low dimensions ( $d_1$  and  $d_2$ ), while firms purchasing products (nondurables, durables, manufacturing chemicals, equipment, wholesale) are concentrated in the manifold with highest dimension  $d_4$ . The manifold with intrinsic dimension  $d_3$  mostly includes firms in the financial and health care sectors. Different dimensions are not only related to the classification of the firm, but also to their financial robustness. We consider the S&P quality ratings for the firms assigned to each manifold (also from Compustat; ratings are available for 2894 firms). In Fig. 5(bottom) we show the distribution of ratings for the different manifolds. These distributions appear to be different. In particular, companies belonging to manifolds of lower dimensions exhibit worse ratings. We suggest a simple interpretation for this phenomenon: a low ID may imply a more rigid balance structure, which may entail a higher sensitivity to market shocks which, in turn, may trigger domino effects in contagion processes. This result shows that a close proxy of the S&P rating can be derived using only topological properties of the data landscape, without any in-depth financial analysis. For example, no information on the commercial relationship between the firms or on the nature of their business is used.

## **Discussion**

The increasing availability of large amount of data has considerably expanded the opportunities and challenges for unsupervised data analysis. Often data come in the form of a completely uncharted "point cloud" for which no model is at hand. A primary goal of the analyst is to uncover some structure within the data. For this purpose, a typical approach is dimensionality reduction, whereby the data are simplified by projecting them onto a low-dimensional space.

The appropriate *intrinsic dimension (ID)* of the space onto which one should project the data is not constant everywhere. In this work we developed an algorithm (Hidalgo) to find manifolds of different ID in the data. Applying Hidalgo, we observed large variations of the ID in datasets of diverse origin (a molecular dynamics simulation, a set of time series from brain imaging, a dataset of firm balance sheets). This finding suggests that a highly non-uniform ID is not an oddity, but a rather common feature. Generally speaking, ID variations can be expected whenever the system under study can be in different "states" corresponding to different degrees of freedom, for instance due to a difference in constraints. For instance, the folded state the protein is able to locally explore the phase space in many independent directions, while in the unfolded state it only performs wider movements fewer directions. In the case of companies, a financially stable company may have more degrees freedom to adjust its balance sheet.

In the cases we analyzed, regions of different dimension were found to host data points differing in important properties. Thus, variations of the ID within a dataset can be used to classify the data into different categories. It is remarkable that such classification is achieved by looking at a simple topological property, the local ID. Let us stress that ID-based classification should not be considered an alternative to clustering methods. In fact, in most cases (e.g., most classical benchmark sets for clustering), different clusters do not correspond to significantly different intrinsic dimensions - rather, they correspond to regions of high density of points within a single manifold of well-defined ID. In such cases, clusters cannot be identified as different manifolds by Hidalgo. Conversely, when the ID is variable, regions of different ID do not necessarily correspond to clusters in the standard meaning of the word: they may or may not correspond to regions of high density of points. A typical example could be that of protein folding: while the folded configurations are quite similar to one another, and hence constitute a cluster in the traditional sense, the unfolded configurations may be very heterogeneous, hence quite far in data space and then not a "cluster" in the standard meaning of the word.

The idea that ID may vary in the same data is not new. In fact, many works have discussed the possibility of a variable ID and developed methods to estimate multiple IDs<sup>7-18,20-22</sup>. Our method builds on these previous contributions but is designed with the specific goal of overcoming technical limitations of other available approaches, and *make ID-based classification a general purpose tool*. Our scheme uses only the distances between the data points, and not their coordinates, which significantly enlarges its scope of applicability. Moreover, the scheme uses only the distances between a point and its  $q$  nearest neighbours, with  $q \leq 5$ . We thus circumvent the notoriously difficult problem of defining a globally meaningful metric<sup>3</sup>, only needing a

consistent metric on a small local scale. Finally, Hidalgo is not hindered by density variations or curvature. For this reasons, Hidalgo is competitive with other manifold learning and variable ID estimation methods, and in particular can yield better ID estimates and manifold reconstruction. We have compared our method with two state-of-the art methods in the literature, considering the same 5-manifold example as in fig. 2. The results of the comparison are presented in Table 1 and in Figure S2. The first method is the local ID estimation by Carter et al.<sup>10</sup>, which combines ID estimation and local smoothing to produce an integer ID estimate for each point. The method cannot correctly discriminate the manifolds of dimension 1 and 4, and yields imprecise estimates of the ID in the two manifolds of dimension 5 and 9. The second method we considered is the “sparse manifold clustering and embedding” (SMCE, Ref.<sup>19</sup>). The method connects neighboring points on the same manifolds in a graph, and then uses spectral clustering on this graph to retrieve manifolds. This method merges the manifolds of dimension 5 and 9 and cannot retrieve the manifold of dimension 4; furthermore, it yields poor dimension estimates. For both methods, the NMI between the ground truth and the assignment is significantly lower than Hidalgo (0.74 and 0.66 compared to 0.83 for Hidalgo). By virtue of the linear structure of Gibbs sampling, Hidalgo is computationally efficient, and therefore suitable for

Ground truth	This work	Ref. <sup>10</sup>	Ref. <sup>19</sup>
d=1 N=1000	d=0.9 N=991	d=1 N=1424	d=2 N=1055
d=2 N=1000	d=2.2 N=965	d=2 N=1135	d=2 N=1249
d=4 N=1000	d=3.8 N=1042	d=3 N=379	not found
d=5 N=1000	d=5.2 N=1003	d=4-5 N=1066	d=4 N=2016
d=9 N=1000	d=8.5 N=999	d=7,8 N=976	merged with d=5
<b>NMI</b>	0.83	0.74	0.66

**Table 1.** Comparison between the performances of Hidalgo, and of the approaches from Refs.<sup>10</sup> and<sup>19</sup> on the dataset with five curved manifolds of Figure 2. We show the estimated value of  $d$  and the number of points assigned to the correct manifold.

the analysis of large data sets. For example, it takes 30 mins to perform the analysis of the neuroimaging data, which includes 30000 data points, on a standard computer using a single core. Implementing the algorithm with parallel Gibbs sampling<sup>36</sup> may considerably reduce computing time and then yield a fully scalable method. Obviously, Hidalgo has some limitations. Some are intrinsic to the way the data are modeled. Hidalgo is not suitable to cover cases in which the ID is a continuously varying parameter<sup>21</sup>, or in which sparsity is so strong that points cannot be assumed to be sampled from a continuous distribution. In particular, Hidalgo is not suitable for discrete data for which the basic assumptions of the method are violated. Others are technical issues related with the estimation procedure, and, at least in principle, susceptible of improvement in refined versions of the algorithm. Finally, let us point out some further implications of our work. Our findings suggest a caveat with respect to common practices of dimensionality reduction, which assume a uniform ID. In case of significant variations, a global dimensionality reduction scheme may become inaccurate. In principle, the partition in manifolds obtained with Hidalgo may be the starting point for using standard dimensionality reduction schemes. For example, one can imagine to apply PCA<sup>1</sup> or Isomap<sup>3</sup>, or sketchmap<sup>37</sup> separately to each manifold. However, we point out that a feasible scheme to achieve this goal does not come as an immediate byproduct of our method. Once a manifold with given ID is identified, it is highly non trivial to provide a suitable parametrization thereof, especially because the manifolds may be highly nonlinear, and even topologically non-trivial. How to suitably integrate our approach with a dimensionality reduction scheme remains a topic for further research. Another implication is that a simple topological invariant, the ID, can be very a powerful tool for unsupervised data analysis, lending support to current efforts at characterizing topological properties of the data<sup>38,39</sup>.

## References

1. Jolliffe, I. T. Principal component analysis and factor analysis. In *Principal component analysis*, 115–128 (Springer, 1986).
2. Roweis, S. T. & Saul, L. K. Nonlinear dimensionality reduction by locally linear embedding. *science* **290**, 2323–2326 (2000).
3. Tenenbaum, J. B., De Silva, V. & Langford, J. C. A global geometric framework for nonlinear dimensionality reduction. *science* **290**, 2319–2323 (2000).

4. Grassberger, P. & Procaccia, I. Measuring the strangeness of strange attractors. In *The Theory of Chaotic Attractors*, 170–189 (Springer, 2004).
5. Levina, E. & Bickel, P. J. Maximum likelihood estimation of intrinsic dimension. In *Advances in neural information processing systems*, 777–784 (2005).
6. Rozza, A., Lombardi, G., Ceruti, C., Casiraghi, E. & Campadelli, P. Novel high intrinsic dimensionality estimators. *Mach. learning* **89**, 37–65 (2012).
7. Barbará, D. & Chen, P. Using the fractal dimension to cluster datasets. In *Proceedings of the sixth ACM SIGKDD international conference on Knowledge discovery and data mining*, 260–264 (ACM, 2000).
8. Gionis, A., Hinneburg, A., Papadimitriou, S. & Tsaparas, P. Dimension induced clustering. In *Proceedings of the eleventh ACM SIGKDD international conference on Knowledge discovery in data mining*, 51–60 (ACM, 2005).
9. Costa, J. A., Girotra, A. & Hero, A. Estimating local intrinsic dimension with k-nearest neighbor graphs. In *Statistical Signal Processing, 2005 IEEE/SP 13th Workshop on*, 417–422 (IEEE, 2005).
10. Carter, K. M., Raich, R. & Hero III, A. O. On local intrinsic dimension estimation and its applications. *IEEE Transactions on Signal Process.* **58**, 650–663 (2010).
11. Campadelli, P., Casiraghi, E., Ceruti, C., Lombardi, G. & Rozza, A. Local intrinsic dimensionality based features for clustering. In *International Conference on Image Analysis and Processing*, 41–50 (Springer, 2013).
12. Johnsson, K., Sonesson, C. & Fontes, M. Low bias local intrinsic dimension estimation from expected simplex skewness. *IEEE Transactions on Pattern Analysis & Mach. Intell.* 1–1 (2015).
13. Mordohai, P. & Medioni, G. G. Unsupervised dimensionality estimation and manifold learning in high-dimensional spaces by tensor voting. In *IJCAI*, 798–803 (2005).
14. Haro, G., Randall, G. & Sapiro, G. Translated poisson mixture model for stratification learning. *Int. J. Comput. Vis.* **80**, 358–374 (2008).
15. Souvenir, R. & Pless, R. Manifold clustering. In *Computer Vision, 2005. ICCV 2005. Tenth IEEE International Conference on*, vol. 1, 648–653 (IEEE, 2005).
16. Wang, Y., Jiang, Y., Wu, Y. & Zhou, Z.-H. Multi-manifold clustering. In *Pacific Rim International Conference on Artificial Intelligence*, 280–291 (Springer, 2010).
17. Goh, A. & Vidal, R. Segmenting motions of different types by unsupervised manifold clustering. In *Computer Vision and Pattern Recognition, 2007. CVPR'07. IEEE Conference on*, 1–6 (IEEE, 2007).
18. Vidal, R. Subspace clustering. *IEEE Signal Process. Mag.* **28**, 52–68 (2011).
19. Elhamifar, E. & Vidal, R. Sparse manifold clustering and embedding. In *Advances in neural information processing systems*, 55–63 (2011).
20. Elhamifar, E. & Vidal, R. Sparse subspace clustering: Algorithm, theory, and applications. *IEEE transactions on pattern analysis machine intelligence* **35**, 2765–2781 (2013).
21. Amsaleg, L. *et al.* Estimating local intrinsic dimensionality. In *Proceedings of the 21th ACM SIGKDD International Conference on Knowledge Discovery and Data Mining*, 29–38 (ACM, 2015).
22. Faranda, D., Messori, G. & Yiou, P. Dynamical proxies of north atlantic predictability and extremes. *Sci. reports* **7**, 41278 (2017).
23. Facco, E., d’Errico, M., Rodriguez, A. & Laio, A. Estimating the intrinsic dimension of datasets by a minimal neighborhood information. *Sci. reports* **7**, 12140 (2017).
24. Xiao, R., Zhao, Q., Zhang, D. & Shi, P. Data classification on multiple manifolds. In *Pattern Recognition (ICPR), 2010 20th International Conference on*, 3898–3901 (IEEE, 2010).
25. Goldberg, A., Zhu, X., Singh, A., Xu, Z. & Nowak, R. Multi-manifold semi-supervised learning. In *Artificial Intelligence and Statistics*, 169–176 (2009).
26. Richardson, S. & Green, P. J. On bayesian analysis of mixtures with an unknown number of components (with discussion). *J. Royal Stat. Soc. series B (statistical methodology)* **59**, 731–792 (1997).
27. Casella, G. & George, E. I. Explaining the gibbs sampler. *The Am. Stat.* **46**, 167–174 (1992).
28. Diebolt, J. & Robert, C. P. Estimation of finite mixture distributions through bayesian sampling. *J. Royal Stat. Soc. Ser. B (Methodological)* **56**, 363–375 (1994).

29. Allegra, M. *et al.* Brain network dynamics during spontaneous strategy shifts and incremental task optimization. *bioRxiv* DOI: [10.1101/481838](https://doi.org/10.1101/481838) (2018). <https://www.biorxiv.org/content/early/2018/11/28/481838.full.pdf>.
30. Allegra, M. *et al.* fmri single trial discovery of spatio-temporal brain activity patterns. *Hum. brain mapping* **38**, 1421–1437 (2017).
31. Lindorff-Larsen, K., Piana, S., Dror, R. O. & Shaw, D. E. How fast-folding proteins fold. *Science* **334**, 517–520 (2011).
32. Huettel, S. A., Song, A. W., McCarthy, G. *et al.* *Functional magnetic resonance imaging*, vol. 1 (Sinauer Associates Sunderland, MA, 2004).
33. Poldrack, R. A., Mumford, J. A. & Nichols, T. E. *Handbook of functional MRI data analysis* (Cambridge University Press, 2011).
34. Schuck, N. W. *et al.* Medial prefrontal cortex predicts internally driven strategy shifts. *Neuron* **86**, 331–340 (2015).
35. Fama, E. F. & French, K. R. Industry costs of equity. *J. financial economics* **43**, 153–193 (1997).
36. Gonzalez, J., Low, Y., Gretton, A. & Guestrin, C. Parallel gibbs sampling: From colored fields to thin junction trees. In *Proceedings of the Fourteenth International Conference on Artificial Intelligence and Statistics*, 324–332 (2011).
37. Ceriotti, M., Tribello, G. A. & Parrinello, M. Simplifying the representation of complex free-energy landscapes using sketch-map. *Proc. Natl. Acad. Sci.* **108**, 13023–13028 (2011).
38. Carlsson, G. Topology and data. *Bull. Am. Math. Soc.* **46**, 255–308 (2009).
39. Zomorodian, A. & Carlsson, G. Computing persistent homology. *Discret. & Comput. Geom.* **33**, 249–274 (2005).

#### **Data availability**

Figure 1, 2, 6 and 7 have raw simulated data. Figure 3,4,5 use real data. All data used are publicly available in the following github repository: <https://github.com/micheleallegra/Hidalgo>

#### **Code availability**

Code is publicly available in the following github repository: <https://github.com/micheleallegra/Hidalgo>

#### **Acknowledgements**

MA acknowledges the FLAG-ERA Project Brainsynch-Hit for providing financial support for his research during completion of this work. We thank Giovanni Barone Adesi and Julia Reynolds (Institute of Finance, USI, Lugano, Switzerland) for helping us with the Compustat dataset and offering precious suggestions for its analysis. We thank Giulia Sormani (SISSA, Trieste, Italy) for suggesting, and providing us with the protein dynamics data. We thank Alex Rodriguez (SISSA, Trieste, Italy) for helping with the analysis of protein data. M.A. thanks the SISSA community at large for the substantial moral and intellectual support received, which has been critical for completion of this work.

The authors declare that they have no competing financial interests.

Correspondence and requests for materials should be addressed to A.L. (email: [laio@sissa.it](mailto:laio@sissa.it)) and A.M.. (email: [antionetta.mira@usi.ch](mailto:antionetta.mira@usi.ch)).

## Supplementary Materials

**Enforcing neighborhood uniformity.** In our model, we wish to obtain well separated manifolds. We do not wish to impose this condition in the form of a rigid constraint, since in real cases regions with different ID are not completely separated, but only as a “soft constraint”, privileging configurations of  $z$  such that the first neighbors of each point are preferentially assigned to the same manifold. In a Bayesian framework, this means that given that  $j$  is among the first neighbors of  $i$ , the probability that  $z_i = z_j$  is increased. Consider the *neighbor matrix*  $\mathcal{N}_{ij}^{(q)}$  defined as:

$$\mathcal{N}_{ij}^{(q)} = \begin{cases} 1 & \text{if } j \neq i \text{ is among the first } q \text{ neighbors of } i \\ 0 & \text{otherwise, including } i = j \end{cases} \quad (6)$$

Intuitively, we would like to impose

$$P_{\text{post}}(z_i = z_j | \mathcal{N}_{ij}^{(q)} = 1, \mu, p) > P_{\text{post}}(z_i = z_j | \mathcal{N}_{ij}^{(q)} = 0, \mu, p). \quad (7)$$

However, Eq. 7 is a relation between posterior probabilities, hence it cannot be directly embedded in the likelihood. What we can specify in the likelihood is the probability of observing the data  $\mathcal{N}_{ij}^{(q)}$ , given an assignment  $z$  of the points. The way to enforce Eq. 7 is assuming that *the first neighbors of each point are preferentially points of the same manifold*. Consider the  $i$ -th row of the neighbor matrix,  $\mathcal{N}_i^{(q)} \equiv \{\mathcal{N}_{ij}^{(q)}, j = 1, \dots, N\}$ .  $\mathcal{N}_i^{(q)}$  is a vector containing  $q$  ones and  $N - q$  zeros. Without any assumption, all configurations of  $q$  zeros and  $N - q$  ones are equally likely. Instead, we assume that neighbors are preferentially points from the same manifold. Formally, we assume that neighbors are selected from the points of the same manifold with probability  $\zeta$  and from a different manifold with probability  $1 - \zeta$ , with  $\zeta > 1/2$ . Correspondingly, we introduce a new term in the likelihood:

$$\mathcal{L}(\mathcal{N}_i^{(q)} | z) = \frac{\zeta^{n_i^{\text{in}}(z)} (1 - \zeta)^{q - n_i^{\text{in}}(z)}}{\mathcal{Z}(\zeta, N_{z_i})}, \quad (8)$$

where

$$n_i^{\text{in}}(z) = \sum_j \mathcal{N}_{ij}^{(q)} \mathbb{I}_{z_j = z_i} \quad (9)$$

is the number of neighbors of  $i$  sampled from the same manifold, and

$$q - n_i^{\text{in}}(z) = \sum_j \mathcal{N}_{ij}^{(q)} \mathbb{I}_{z_j \neq z_i} \quad (10)$$

is the number of neighbors of  $i$  sampled from a different manifold. Function  $\mathcal{Z}$  is a normalization factor that depends on  $\zeta$ :

$$\mathcal{Z}(\zeta, N_{z_i}) = \sum_{\{\mathcal{N}_i^{(q)}\}} \zeta^{n_i^{\text{in}}(z)} (1 - \zeta)^{q - n_i^{\text{in}}(z)}. \quad (11)$$

and can be expressed in a compact way as

$$\mathcal{Z}(\zeta, N_{z_i}) = (1 - \zeta)^q \binom{N - N_{z_i}}{q} {}_2F_1\left(-q, 1 - N_{z_i}, N - N_{z_i} - q, \frac{\zeta}{1 - \zeta}\right), \quad (12)$$

where  ${}_2F_1(a, b, c, x)$  is the hypergeometric function. The derivation of this expression and the details about the likelihood term in (8) are presented below. By considering all points  $i$ , we obtain the global likelihood

$$\mathcal{L}(\mathcal{N}^{(q)} | z, \zeta) = \prod_i \mathcal{L}(\mathcal{N}_i^{(q)} | z, \zeta) = \prod_k \frac{\zeta^{n_k^{\text{in}}} (1 - \zeta)^{q N_k - n_k^{\text{in}}}}{\mathcal{Z}(\zeta, N_k)^{N_k}} \quad (13)$$

where

$$n_k^{\text{in}} = \sum_{ij} \mathcal{N}_{ij}^{(q)} \mathbb{I}_{z_i = k} \mathbb{I}_{z_j = k} \quad (14)$$

is the total number of “internal” neighbors of points from manifold  $k$  and

$$n_k^{out} = \sum_{ij} \mathcal{N}_{ij}^{(q)} \mathbb{I}_{z_i=k} (1 - \mathbb{I}_{z_j=k}) = qN_k - n_k^{in} \quad (15)$$

is the total number of “external” neighbors of points from  $k$ . Note that since  $\mathcal{Z}$  depends on  $i$  only through the hidden variables  $z$  we are able to split the product into  $K$  components.

With this additional term in the likelihood, we obtain

$$\frac{P_{post}(z_i = z_j | \mathcal{N}_{ij}^{(q)} = 1, \boldsymbol{\mu}, p)}{P_{post}(z_i = z_j | \boldsymbol{\mu}, p)} = \frac{\zeta}{1 - \zeta} > 1/2$$

**Derivation of the neighborhood uniformity term.** With reference to  $\mathcal{N}_i^{(q)}$ , without any assumption, all configurations containing  $q$  zeros and  $N - q$  ones are equally likely. It is easy to compute the number of such configurations. The problem is analogous to the problem of selecting  $q$  balls from a box containing  $N - 1$  balls: we have to choose  $q$  neighbors among  $N - 1$  points, point  $i$  being excluded. The number of possible choices is  $\binom{N-1}{q}$ . Hence, all configurations of  $\mathcal{N}_i^{(q)}$  being equally likely we would have

$$\mathcal{L}(\mathcal{N}_i^{(q)}|z) = \binom{N-1}{q}^{-1}, \quad \forall i.$$

Instead, we assume that the neighbors of a point are preferentially points from the same manifold. Formally, we assume that neighbors are selected with probability  $\zeta$  among the  $N_{z_i}$  points assigned to the same manifold of  $i$ , and with probability  $1 - \zeta$  among the  $N - N_{z_i}$  points assigned to a different manifold. Here  $\zeta > 1/2$ , so that configurations with neighbors assigned to the same manifold are more likely. Now, the problem is analogous to the problem where we have to select  $q$  balls from two boxes, a black box containing  $N_b$  balls and a white one containing  $N_w$  balls. Before selecting each ball, we choose the box, the black one with probability  $\zeta$  and the white one with probability  $1 - \zeta$ . Clearly, the probability of a choice with  $n_b$  black and  $q - n_b$  white balls is then proportional to  $\zeta^{n_b}(1 - \zeta)^{q - n_b}$ . For a given  $n_b$ , the number of possible choices of balls is

$$\binom{N_b}{n_b} \binom{N_w}{q - n_b}$$

One can easily verify that  $\sum_{n_b=0}^q \binom{N_b}{n_b} \binom{N_w}{q - n_b} = \binom{N_b + N_w}{q}$ . The probability of a given choice is then

$$\frac{\zeta^{n_b}(1 - \zeta)^{q - n_b}}{\mathcal{Z}}$$

where  $\mathcal{Z} = \sum_{n_b=0}^q \binom{N_b}{n_b} \binom{N_w}{q - n_b} \zeta^{n_b}(1 - \zeta)^{q - n_b}$ . By using the formula (Abramowitz and Stegun, 15.4.1)

$${}_2F_1(-m, b, c, z) = \sum_{n=0}^m (-)^n \binom{m}{n} \frac{(b)_n}{(c)_n} z^n$$

where  $(a)_n = a(a + 1) \dots (a + n - 1)$  is the Pochhammer symbol and doing some simple algebra,  $\mathcal{Z}$  can be compactly expressed as

$$\mathcal{Z} = (1 - \zeta)^q \binom{N_w}{q} {}_2F_1(-q, -N_b, N_w - q, \frac{\zeta}{1 - \zeta}).$$

Substituting  $N_b$  with  $N_{z_i} - 1$  (the number of points assigned to the same manifold as  $i$ , excluding  $i$ ),  $N_w$  with  $N - N_{z_i}$  (the number of points assigned to a different manifold), and  $n_b$  with  $n_i^{in}$ , we obtain the likelihood of a given configuration of  $\mathcal{N}_i^{(q)}$  as

$$\mathcal{L}(\mathcal{N}_i^{(q)}|z, \zeta) = \frac{\zeta^{n_i^{in}(z)}(1 - \zeta)^{q - n_i^{in}(z)}}{(1 - \zeta)^q \binom{N - N_{z_i}}{q} {}_2F_1(-q, 1 - N_{z_i}, N - N_{z_i} - q, \frac{\zeta}{1 - \zeta})}.$$

**Choice of the free parameters.** In order to find a good configuration for the parameters  $(q, \zeta)$ , we perform tests with several values of  $q \in \{2, 3, \dots, 20\}$  and  $\zeta \in [0.5, 1)$ . We focus on the most challenging case, the one of two Gaussians in dimensions 4 and 5. The crucial figure of merit to assess the performance of the method is the mutual information between the estimated and the true assignment of  $z$ , which measures the quality of the assignment of points to manifolds. Indeed, once the manifolds are correctly separated, the problem is essentially reduced to a dimension estimation within the single manifolds (which is successfully solved by TWO-NN). In supplementary Fig. 6 we show the MI as a function of  $(q, \zeta)$  for a Gibbs sampling with  $10^5$  iterations. For most values of  $q$ , the MI first increases, then decreases with  $\zeta$ . This can be expected on the basis of the following considerations. When  $\zeta$  is close to 0.5, as we discussed above, the method cannot discriminate different manifolds. When  $\zeta$  is increased, the posterior distribution starts to prefer configurations that approximately satisfy the neighborhood homogeneity constraint. For sufficiently high  $\zeta$ , the posterior distribution is sharply peaked at the configuration that optimally satisfies this constraint; correspondingly, if the Gibbs sampler is able to explore the parameter space exhaustively, it will eventually find this peaked region and remain trapped there. Hence, the MI achieves average values close to 1. However, for  $\zeta$  close to 1, the posterior distribution is very likely to also have pronounced local maxima and, depending on the initial configuration, the sampler may remain trapped in one of them. Hence, one can observe a drop in the MI. In general these sampling issues can be worsened when  $q$  is increased since the local maxima become more and more pronounced. In principle, this problem may be dealt with by resorting to well established enhanced sampling techniques. For simplicity, in the present work we prefer to verify that there is a region of the parameter space where the results appear stable, and restrict to this regions for subsequent analyses.

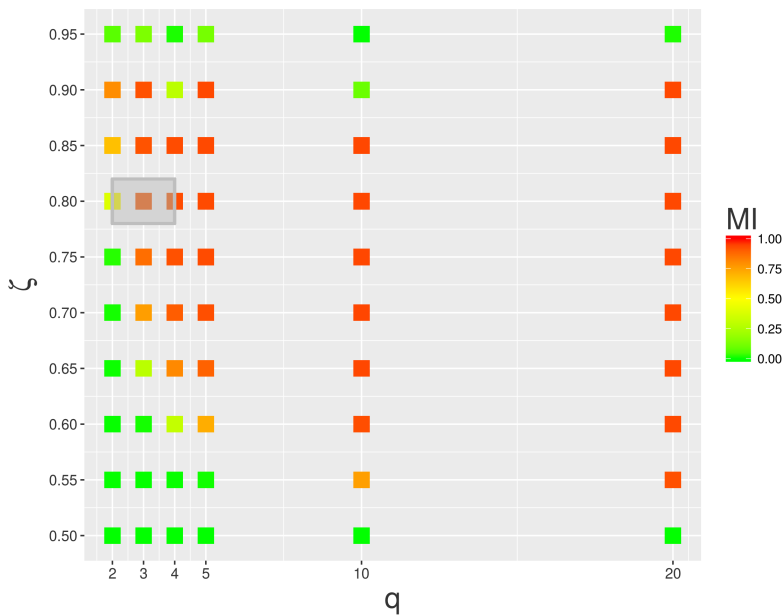


**Figure 6. Choice of free parameters**

**Compustat variables used.**

#	Variable	#	Variable	#	Variable
1	Acquisitions	12	Liabilities - Total	23	Interest and Related Expense - Total
2	Assets - Total	13	Net Income (Loss)	24	Goodwill
3	Capital Expenditures	14	Operating Income Before Depreciation	25	Intangible Assets - Total
4	Cash	15	Property Plant and Equipment - Total (Net)	26	Pretax Income
5	Common Shares Outstanding	16	Purchase of Common and Preferred Stock	27	Pretax Income - Foreign
6	Common/Ordinary Shareholders	17	Sales/Turnover (Net)	28	Investment and Advances - Equity
7	Debt in Current Liabilities - Total	18	Stockholders Equity - Parent	29	Investment and Advances - Other
8	Long-Term Debt - Total	19	Income Taxes Paid	30	Increase in Investments
9	Cash Dividends (Cash Flow)	20	Research and Development Expense	31	Sale of Investments
10	Earnings Before Interest and Taxes	21	Price Close - Annual - Fiscal		
11	Employees	22	Preferred/Preference Stock (Capital) - Total		

**Table 2. Compustat variables used**

### Comparison with other methods.

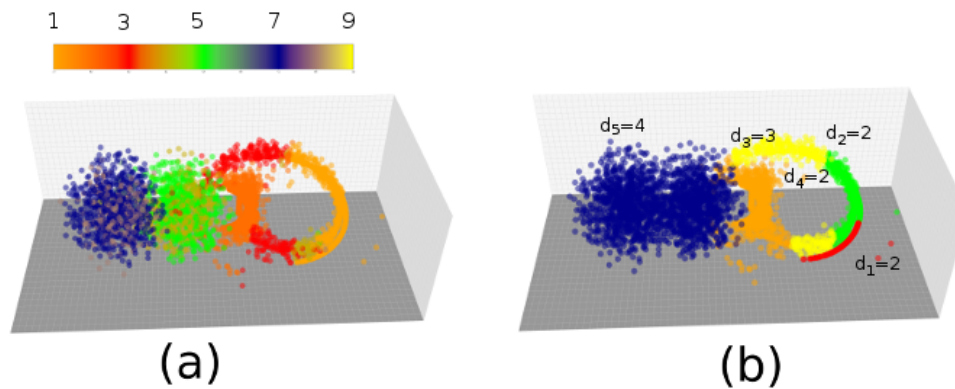


**Figure 7. Results of other variable-ID analysis methods on topologically complex artificial data.** We considered sets of points drawn from mixtures of multivariate Gaussians embedded in curved nonlinear manifolds, as detailed in fig. 2 In panel a) we show the local ID estimates given by the method of Carter et al.<sup>10</sup>, considering  $k = 50$  nearest neighbors for local ID estimation and smoothing. The method assigns an integer dimension to each point: in the plot, the dimension of each point is represented by its color, according to the color bar shown. The method correctly retrieves the manifolds of dimension 5 and 9, even though the points in the manifold with dimension 5 are assigned a local ID that oscillates between 4 and 5, and points in the manifold with dimension 9 are assigned a local id that oscillates between 7 and 8. Also the manifold of dimension 2 is well identified. The manifolds of dimension 1 and 4, however, cannot be correctly discriminated. Points of the manifold of dimension 4 are assigned ID estimates of 1 or 3, without a clear separation of the manifolds. The NMI between the ground truth and the assignment, assuming that points with the same (integer) local ID form a separate cluster, is 0.74. In panel b) we show the assignment of points as given by the SMCE method<sup>19</sup>. The manifolds of dimension 5 and 9 are merged. The manifold of dimension 2 is identified, but it is also contaminated by points from the manifold of dimension 4. SMCE cannot correctly retrieve the manifolds of dimension 1 and 4. The NMI between the ground truth and the assignment is 0.66. ID estimates obtained according to the prescription given in<sup>19</sup> are largely incorrect.